Trabajo Fin de Grado
Grado en Ingeniería en Tecnologías Industriales - Intensificacíon energética

Thermal analysis of the FILD head in the ASDEX Upgrade Tokamak

Autor: Javier Hidalgo Salaverri

Tutor: Manuel Toscano Jiménez

Tutor: Juan Manuel Ayllón Guerola

Dpto. Física Aplicada III
Escuela Técnica Superior de Ingeniería
Universidad de Sevilla

Sevilla, 2018

Trabajo Fin de Grado

Grado en Ingeniería en Tecnologías Industriales -
Intensificacíon energética

Thermal analysis of the FILD head in the ASDEX Upgrade Tokamak

Autor:

Javier Hidalgo Salaverri

Tutor:

Manuel Toscano Jiménez

Profesor Titular de Universidad

Tutor:

Juan Manuel Ayllón Guerola

Profesor Invitado

Dpto. Física Aplicada III

Escuela Técnica Superior de Ingeniería

Universidad de Sevilla

Sevilla, 2018

Trabajo Fin de Grado: Thermal analysis of the FILD head in the ASDEX Upgrade Tokamak

Autor: Javier Hidalgo Salaverri
Tutor: Manuel Toscano Jiménez
Tutor: Juan Manuel Ayllón Guerola

El tribunal nombrado para juzgar el trabajo arriba indicado, compuesto por los siguientes profesores:

Presidente:

Vocal/es:

Secretario:

acuerdan otorgarle la calificación de:

El Secretario del Tribunal

Fecha:

Agradecimientos

A mi hermano y a mis padres, por escucharme hablar de ingeniería durante cuatro años aunque no me entiendan (y los que quedan) y por su apoyo incondicional.

A María, que ha hecho más llevadera la carrera de fondo del grado.

A mis tutores: Manuel Toscano, por creer en mi y apoyarme durante estos cuatro años y a Juan Manuel Ayllón por recibirme con los brazos abiertos en el mundo de la fusión.

Saber es noche

Abstract

Fusion power is set to be an important energy agent in the mid future. Magnetic confinement fusion is the current most advanced technology for fusion energy. An important fraction of the plasma energy is stored in fast ions, high temperature ions that tend to abandon the magnetic confinement due to different physical phenomena. To be able to make a self sustained fusion (ignition) those fast ions must not escape. The fast Ions Loss Detector (FILD) have been set in numerous Tokamaks to study the behavior of those ions. This work develops a numerical tool in order to simulate the thermal fluxes a FILD will be facing during operation. Particle orbits within a Tokamak were approximated by magnetic field lines for this purpose.

OcTree algorithm and a preliminary analysis of the position of the frontier between wet or dry zones (with or without particle impact) have been implemented to reduce computational time during simulations. As thermal model, the cosine model has been chosen, where the parallel heat flux is taken as dominant and then weighted in function of the intersection angle between magnetic field line and the FILD head.

An example case has been run for one of the FILDs installed in the ASDEX Upgrade Tokamak. This machine is an important ITER physics testing site for its unique divertor configuration, taking advantage of its huge plasma shot library. The thermal analysis for this example case has been carried out using ANSYS software for FILD 4.

The resulting tool comes as highly customizable as the magnetic equilibrium, tokamak, chosen FILD and FILD position are easily exchangeable, making it a good solution for a wide range of configurations.

Contents

List of Figures

List of Tables

1 Introduction

The aim of this work is to develop a flexible tool to study the thermal behavior of fast ions loss detectors under a wide range of circustances. Before entering inside the study of FILD itself an introduction to nuclear fusion, plasma physics, the tokamak reactor and fast ions is needed.

1.1 Nuclear Fusion

Nuclear fusion in a general sense is the collision of two light elements to birth a heavier one liberating a great amount of energy. This requires that the binding energy per nucleon (the energy the nucleus has in order to maintain its inner stability) of the resulting nucleus would be bigger than the lighter ones. This is easily seen in figure 1.1 where the maximum is around the iron (with A = 56), for lighter elements this energy would be generated by fusing two light elements meanwhile for heavier ones, energy would be produced by the fission of a heavy element.

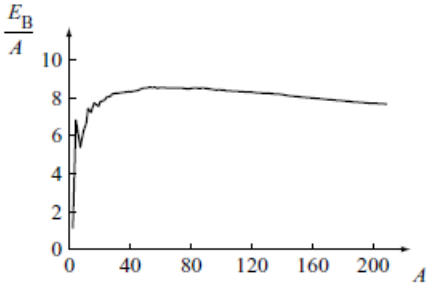

Figure 1.1 Binding energy per nucleon vs. mass number for the dominant form of each chemical element. [1].

Different reactions can be used in order to achieve fusion. As the figure 1.1 suggests the best solution would be to choose the lightest element in order to get the maximum energy

from the reaction. Therefore the focus will be in hydrogen and helium, specifically in the reactions: D-D, D-T and D-He^3 (being D, deuterium and T, tritium) for being those the optimal reactions. In figure 1.2 it is shown the cross section of each of those reactions in function of the kinetic energy of D, in other words, of its temperature. As the figure shows the D-T reaction has the biggest cross section and the lower requirement in terms of temperature. That is the reason behind the election of this reaction as the first to be studied in fusion reactors and, therefore, the one that would be taken into account for now on.

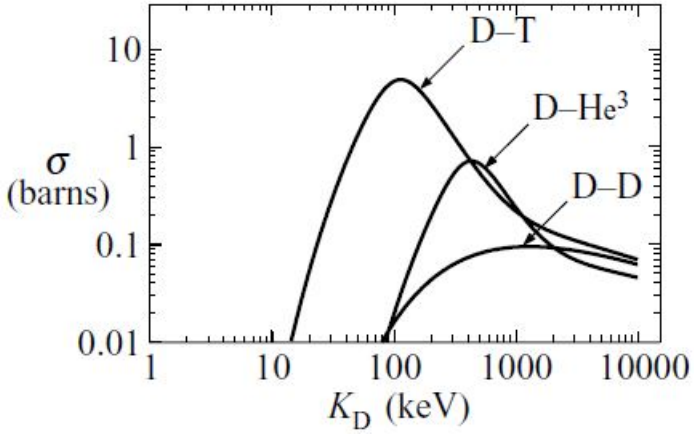

Figure 1.2 Experimentally measured cross sections for the D–T, D–He3, and D–D fusion reactions as a function of deuterium kinetic energy (K_D). [2].

The D-T reaction occurs as:

$$D + T \rightarrow \alpha\,(3.5\,MeV) + n\,(14.1\,MeV) \tag{1.1}$$

This reaction produces around 3.52 MeV/nucleon which translates to the macroscopic world to 338x10^6 MJ/kg. For comparison, the energy released in a U^{235} fission reaction accounts for 0.88 MeV/nucleon and 84x10^6 MJ/kg. But for the fusion to happen it requires around 100 keV (around 100 million K) this means the hydrogen gas will be ionized and therefore it would have become a plasma.

For fusion to take place without any external help (this is, a self sustainable reaction) the Lawson criterion must be accomplished. Lawson criterion (also known as the triple product) gives the conditions were a plasma can exist as a function of its temperature (T), plasma pressure (p) and the confinement time (τ_e) in a simplified way this inequation can be written as [1]:

$$p * \tau_e \geq 0.11 * \frac{T^2}{<\sigma * v>} \tag{1.2}$$

With <σ*v> the average value of the cross-section times the relative velocity.

This criterion opens different ways of approaching fusion plasmas. Depending on how the parameters are chosen the main options are:

- **Gravitational Fusion:** the only fusion source in nature. The problem is addressed with high pressures. Pressures that can only be obtained by the tremendous gravitational forces that are found in the nucleus of a star. Therefore this way of achieving fusion is not in the reach of technology.

- **Inertial Confinement Fusion:** D-T fuel in the form of a 2 mm sphere is highly compressed and then hit by numerous lasers in a brief period reaching temperature of keV. Though the confinement time in this case is very small (in the order of μs), high pressure and specially high energies allow the fusion to happen. [3]

- **Magnetic Confinement Fusion:** D-T fuel is in the form of plasma. It is confined for few seconds thanks to a series of magnetic fields. Temperatures of around 100 kev are achieved thanks to Ohmnic heating and neutral beams between others. To close the triple product the pressure is supplied by the pressure of the own plasma and the one applied by the electromagnetic field. This is the kind of fusion that takes place in the ASDEX Upgrade Tokamak and therefore the one that will be the subject of this work.

1.2 Plasma

Plasma is commonly known for being the forth state of matter. It occurs when a gas is heated to high enough temperature that the atom overcomes its ionization threshold taking place the separation between the ionized nuclei and their electrons. This results to a charged cloud of ions and electrons. For an hydrogen atom to ionize an energy of 13.6 eV [4] must be supplied and as it was stated in the previous section temperatures of 100 keV are needed for the fusion reaction D-T to succeed, so it is assure the mix will be ionized. The fusion therefore occurs when kinetic energy overcomes Coulomb's barrier and strong nuclear forces come into play fusing both nuclei.

Plasma is generally characterized by:

- **Ionized gas:** nuclei and electrons are no longer linked due to the high kinetic energies overcoming the Coulomb attractive forces.

- **Quasi-neutrality:** in a microscopic scale plasma is charged due to the separation between charges caused by the ionization but, if seen macroscopically, it appears to be neutral. This phenomenon occurs because each ion is surrounded by a cloud of electrons with the same absolute charge which gives birth to neutrally charged spheres. These spheres, called Debye's spheres, when translated into the macroscopic world result into an apparently non-charged plasma.

- **Collective behavior:** plasma being an ionized gas is governed by Maxwell's laws, so the electric potential should promote the rapprochement between ions and electrons

due to Coulomb's force. However this is not the case in plasma. As it has already been said before, plasma temperatures are quite high and therefore its kinetic energy will be as well. Comparing kinetic and potential energy means that the potential is neglected against the huge value of kinetic energy, so the effect of Coulomb's force is not enough to join ions and electrons.

The only moment when the potential could overcome the high kinetic energy would be when an electron randomly got close enough to the nucleus making the potential even bigger than kinetic (after all potential energy grows as 1/r) but this situation won't happen often due to the low densities in plasma. Given all of this, the electric density can be represented as a smooth, continuous distribution of electrons and ions and therefore long range interactions along the plasma will occur. [1]

- **High electrical conductivity:** low collisions and high kinetic energy means low resistivity and therefore high conductivity. As the plasma temperature is increased conductivity increases, this is a problem when talking about heating up the plasma as one of the means to do it is by Ohmic heating using the plasma as the secondary of a transformer.

The electromagnetic properties of fusion plasma all together with its high temperatures makes working with it an important challenge both for engineering and for physics.

1.3 Particle motion in plasma

Particles in plasma are affected by an electric and a magnetic field. Suppose first the particle is only affected by an uniform magnetic field, therefore it will have a circular motion in a perpendicular plane to those magnetic field lines as shown in figure 1.3 centered around the called *guiding center*. This movement is characterized by its ciclotronic frequency (ω_c) and its Larmor radius (r_L) or gyroradius:

$$\omega_c = \frac{|q| * B}{m} \tag{1.3}$$

$$r_L = \frac{m * v\perp}{|q| * B} = \frac{v\perp}{\omega_c} \tag{1.4}$$

Particle motion is also commonly represented using the pitch angle, defined as the ratio between the parallel component of the velocity and the total velocity.

$$\Lambda = \frac{v_{||}}{v_t} = cos(\alpha) \tag{1.5}$$

An electric field perpendicular to the magnetic one is added, this means that the particle accelerates so Larmor radius is modified. Due to the presence of both fields a drift happens

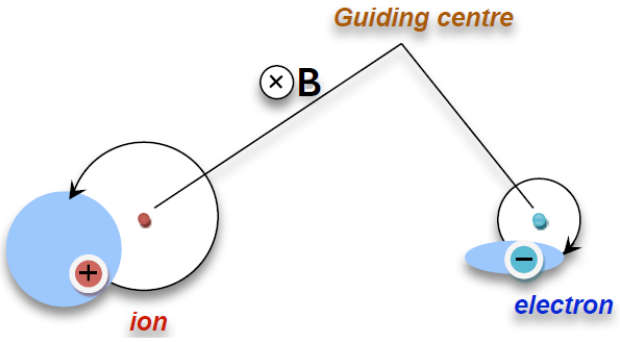

Figure 1.3 Circular motion of a particle in a field line [5].

denoted as ***ExB*** *drift*, shown for ions and electrons in figure 1.4.

$$\vec{v}_d = \frac{\vec{E}x\vec{B}}{B^2} \tag{1.6}$$

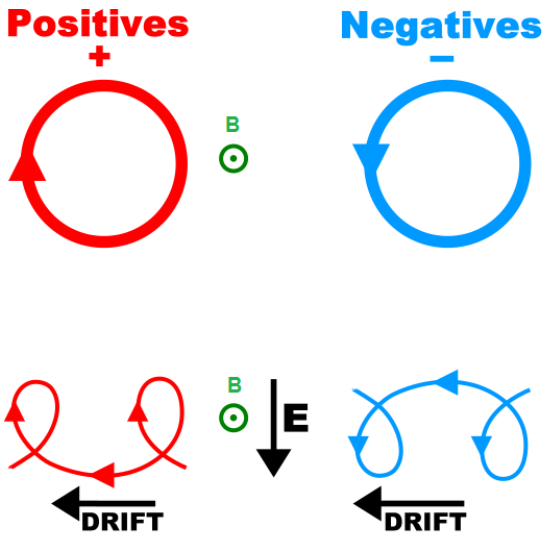

Figure 1.4 ExB drift in ions (left) and electrons (right) [6].

Therefore the real motion will be the sum of the two of them: an helicoidal movement with a guiding center traveling at v_d speed, ρ gyroradius and ω_c ciclotronic frequency [5]. This description of particle motion in plasma is also known as *full orbit*.

1.4 Magnetic confinement

Currently magnetic confinement is the most advanced way of fusion. Even though no Tokamak has been able to produce positive net energy yet, in Cadarache (France) ITER project is being built as the culmination of a world wide project lead by the European Union

with the goal of producing 30 times more energy than the fed to the system. This landmark would demonstrate the technological and physical feasibility of fusion energy as a way of producing commercial energy.

Magnetic confinement takes advantage of the ionized nature of plasma to confine it using a series of powerful magnets. Using this concept two main designs have been raised: Tokamak and Stellarator, both of them toroidal reactors. But before entering in the differences between both designs, why toroidal?

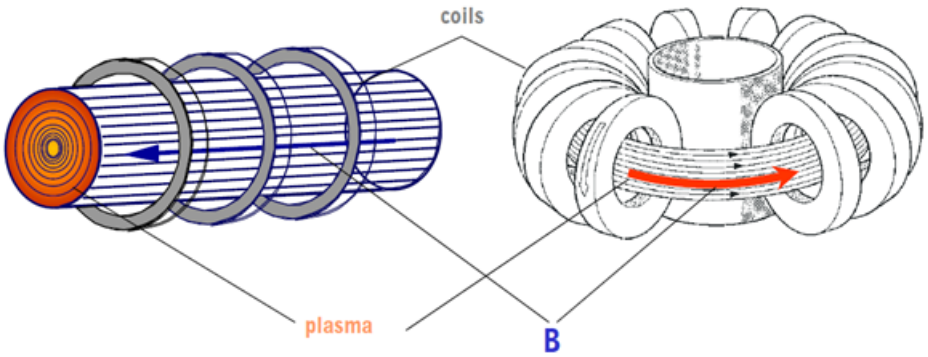

Figure 1.5 Comparison between linear and toroidal confinement in a Tokamak.[7] .

Figure 1.5 shows the difference between linear and toroidal confinement. At first sight a linear fusion device could seem like the best option as the toroidal geometry brings to the table harder challenges for engineers and physicists, indeed this was historically the first design in magnetic confinement. But the problem with this design is that it has some intrinsic losses that are not acceptable. As the device is finite, at the end of it particles will collide with the walls, this would be disastrous not only for the plasma stability but for the walls themselves that would be severely damaged in a few shots. Also in a linear configuration, between two consecutive magnets some of the field lines won't be closed and therefore particles that would follow them won't be confined neither.

These reasons make the toroidal geometry the best option, as it has no ends where the particles could collide (at least if the confinement were ideal) and inside it magnetic field lines are perfectly closed. But toroidal geometry has its own flaws too. With this configuration the distance between two magnets is not constant anymore. In the inner radius magnets will be closer than in the exterior part and therefore as B α1/r, the magnetic field would experience a gradient within that would make the device unsuitable for magnetic confinement. In how this problem is approached is where the difference between Tokamak and Stellarator resides:

- **Tokamak:** Russian design developed in 1956, it is shown in the right part of figure 1.5. The magnets configuration by themselves will produce the magnetic gradient issue but this is fixed by a central solenoid that induces a current in the plasma canceling the magnetic drift. The saturation current of the solenoid has become one of the limiting factors to get higher confinement times in this kind of reactors. Thanks

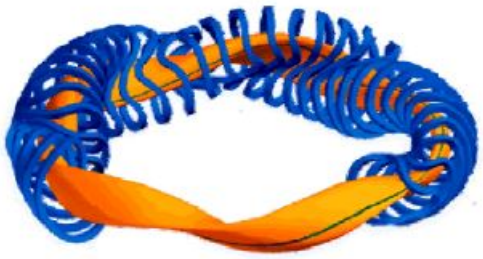

Figure 1.6 Stellarator conceptual design [7].

to its relatively easy geometry, Tokamaks presents axisymmetry which makes its analysis quite easier.

- **Stellarator:** Created by the USA in 1951, represented in figure 1.6. In this case the magnetic drift is solved by the disposition of the own magnets, for this to be accomplish numerical simulations must be run in order to obtain the very complex shapes that each magnet must have. Even though this solves the magnetic drift problem in a clean way (from a purely physics point of view), some other issues are created along the way. The most obvious one is a manufacturing problem that involves serious engineering challenges; the second one passes on the effectivity of the own reaction, the complex geometry of the magnets create little free volume for the plasma and therefore for a given reactor size, Stellarator will have less plasma than a Tokamak. Therefore net positive energetic reactions are harder to obtain with this design. Another problem comes from the changing form of the plasma, which means that there is no axisymmetry and therefore each section will have to be studied separately.

The benefits and problems enumerated for both designs have tip the scale in favor of the Tokamak design that currently is the most advanced solution for nuclear fusion. And therefore will be the design that will be used for ITER as the first try to get to an almost commercial state.

1.5 Tokamak and ASDEX Upgrade

In this section Tokamak characteristics will be defined but with a special focus on the peculiarities of ASDEX Upgrade Tokamak.

As it was explained in the previous section Tokamaks achieve magnetic stability by a series of magnets and a central electrical conductor. Those magnets are positioned in two ways: poloidal magnets and toroidal magnets. In figure 1.7 both directions are defined and also the poloidal magnets are shown, normally toroidal magnets are not depicted in schematic figures as it tend to make figures harder to understand.

Now that toridal and poloidal directions are defined, a description of the general parts of

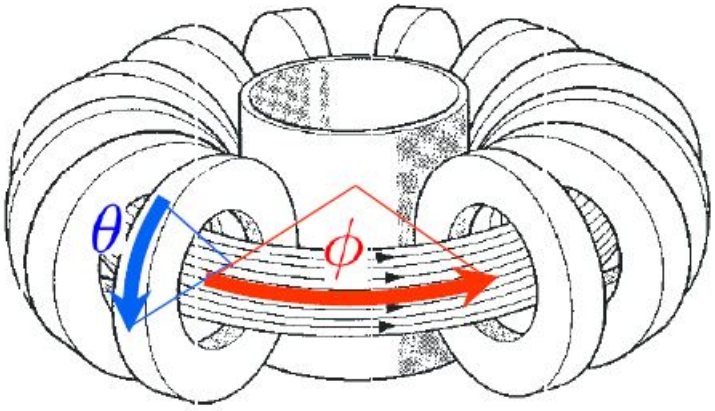

Figure 1.7 Toroidal (Φ) and poloidal (Θ) coordinates in a Tokamak. [7].

a Tokamak can be introduced. As an example, ASDEX Upgrade Tokamak will be used. Special characteristics of ASDEX Upgrade versus normal Tokamak configuration will be pointed when necessary. Actually the figure (1.8) refers to ITER but for the purpose of this explanation there is no difference and therefore we will take it as it was ASDEX Upgrade.

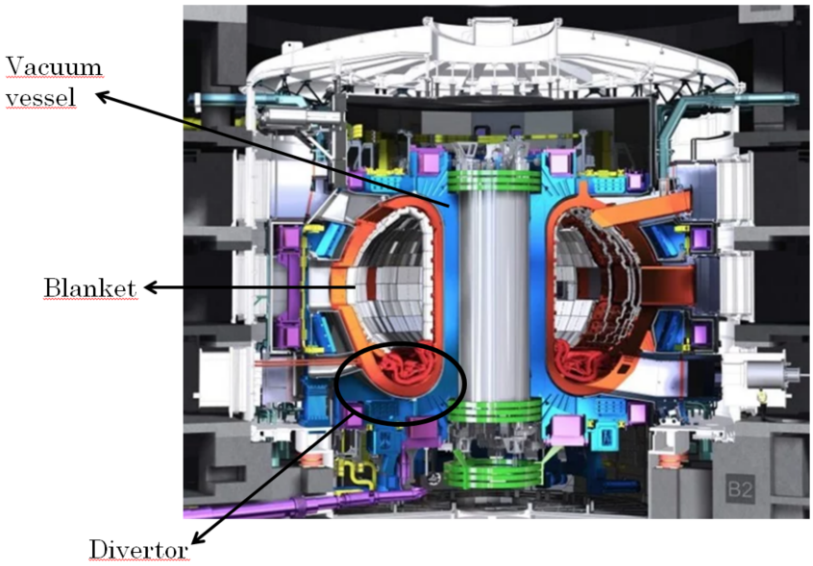

Figure 1.8 Poloidal section of ITER. Structurally similar to ASDEX Upgrade [8].

- **Blanket:** is the first line of defense against the high temperatures of plasma. It is formed by a cover of tiles made of beryllium, tungsten or carbon. Plasma is not always perfectly confined so there are times when it can collide with the so called *first wall* and therefore heat deposition won't only be due to radiation but also for particle collisions (heat model will be discussed in chapter 4). Normally in a Tokamak of a considerable size the heat deposition in the first wall of the blanket can account up to 1-4 MW/m^2.

- **Vacuum vessel:** blanket being a puzzle of tiles makes pretty clear that vacuum could not be maintained within. This is where the vacuum vessel enters in play, as its name says the mission of the vaccum vessel is keeping the inner reactor sealed in order to not let air from the exterior going in which would destroy the vacuum and contaminate the plasma.

- **Divertor:** is the key difference between ASDEX Upgrade and a common Tokamak, it will be also included in ITER from there the importance of ASDEX in the frame of the ITER project. As seen in figure 1.9 magnetic field lines tend to the divertor where they collide. But the particles that normally end colliding along those field lines are impurities of plasma which would hinder the fusion reaction and the heat transfer. In the divertor power densities of $10\ \mathrm{MW/m^2}$ are achieved, a power deposition that in the absence of a divertor would arrive to the blanket.

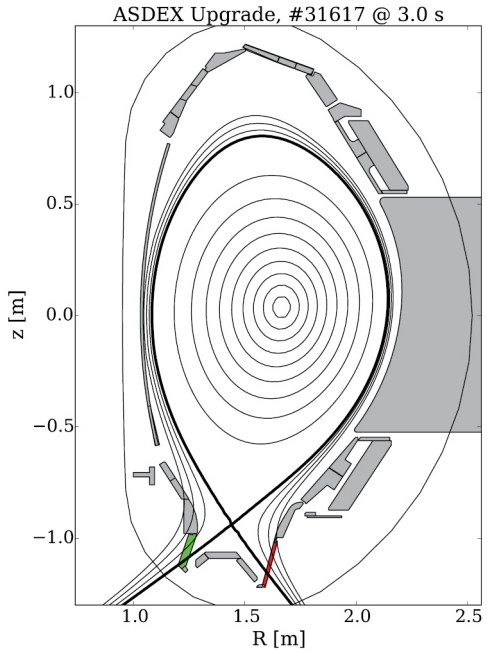

Figure 1.9 Poloidal section of ASDEX Upgrade with magnetic field lines of constant value. [9].

Now that the basis of the Tokamak design are cemented ASDEX (Axially Symmetric Divertor EXperiment) Upgrade, also known as AUG, can be introduced. ASDEX Upgrade, named after its predecessor ASDEX (1980-1990), started its operation in 1991 in the city of Garching, Germnay. The peculiarity of this Tokamak comes from having a divertor that, as it was explained before, is not a common feature in all Tokamaks. Due to the divertor configuration and the geometry of the toroidal coils, ASDEX got the task of preparing all the physics backup needed to start operating ITER, serving as a testing installation for plasma shaping and stability control. Therefore a good understanding of everything that happens in the interior of the Tokamak (with an special emphasis on the divertor) has to be achieved in order to get ITER working as soon as possible and in good conditions. [10]

ASDEX Upgrade has been used to develop this work as its geometry and FILD disposition are known precisely and in a easy-to-work-with way. AUG plasma shot library was also used during this work. Nonetheless other Tokamaks could have been used freely thanks to the modularity of the tool developed in this work

From a technical point of view ASDEX is a 9 meters high D-shaped-toroid with a volume of 13 m^3 divided in eight equal parts. In a general sense, AUG can be classified as a medium size Tokamak but it is the biggest one in Germany. A total of 12 vertical coils are used to control plasma form colliding with inner walls of the vessel. To achieve fusion plasma conditions within, ASDEX uses a magnetic field of 3.9 T. All this makes a total mass of plasma of 3 mg [10]. Five FILDs are installed in ASDEX currently. More technical data can be found in table1.1.

Table 1.1 ASDEX Upgrade technical data [11].

Height	9 m
Major radious	5 m
Total weight	620 T
Number of toroidal coils	16
Number of poloidal coils	12
Maximum magnetic field	3.9 T
Normal magnetic field	2.5 T
Main material of the first wall	Carbon + Tungsten
Plasma current	0.6 - 1.4 MA
Shot duration	<10 s
Plasma heating	<27 MW
Ohmic heating	1 MW
NBI heating	20 MW
Radiofrequency heating (ions)	7 MW
Radiofrequency heating (electrons)	3.5 MW

1.6 Fast ions

Fast ions are ions whose temperature is greater than the average one within a plasma. Qualitatively they are faster than thermal ions (non-excited ions) and slower than thermal electrons: $v_i<v_f<_e$ also their gyroradius is the largest one: $\rho_f<\rho_i<\rho_e$. Due to this, their behavior in an electromagnetic field will be different from the shown by a thermal particle [12].

Fast ions are normally found in the center of the plasma, where the highest temperatures are. Particle velocity follows a maxwellian distribution where the right zone represent those fast ions. Therefore fast ions will be the result of increasing the overall plasma temperature, this can happen due to several processes [13] :

- **D-T reaction:** in the form of α particles.

- **Ohmic heating:** serves as the first way of heating up plasma, even though is not the main way of producing fast ions, it is a necessary part of it. The central conductor of the Tokamak induces a current in the plasma. This current as a result of Ohm's law heats up the plasma $P = I^2_{plasma} * R_{plasma}$. This heating method is limited by the resistivity of plasma is a function of $T^{-3/2}$. So when plasma temperature rises the efficiency of Ohmic heating goes down.

- **Neutral Beam Injection (NBI):** a beam of highly energetic neutral particles impact the plasma heating it up. First particles must be charged in order to be accelerated. Once they get energy levels above the plasma temperature (around 10 keV), the beam passes through a low density gas which neutralizes the majority of the beam. The successfully neutralized particles are then injected in the plasma current. It is important using neutrals as they won't be affected by the magnetic field and they will be able to cross the plasma and deposit its energy in the inner plasma. Heating up comes from collisions of the neutral beam with electrons or with charge exchange processes with ions, this second mechanism produces fast ions from the original ions as well as from the old neutral particles. ASDEX counts with 2 NBI systems [13]

- **Radiofrequency (ICRF):** in this very chapter the ciclotronic frequency, the natural frequency of plasma, were defined. If a electromagnetic wave had the same frequency as the ciclotronic frequency or n times that frequency (being n a natural number) then wave and plasma would be in resonance. In resonance heat transfer achieves high efficiency. As a result of the heating up of plasma can be translated into the appearance of new fast ions [13].

For the first two sources the initial energy of the fast ions is defined but for the ICRF it can't be determine [12].

Their high velocities mean they are essential for keeping the high temperatures needed for the fusion reaction. Fast ions being only a 5% of the total plasma density account for 1/3 of its kinetic energy. That is why a good confinement of them is necessary in order to not drastically lose efficiency and to allow the reaction to be self sustained (*ignition*). Also escaping fast ions can produce unexpected damages in the vessel walls and produce more impurities, harming plasma quality until ignition is no longer possible.

Fast ions can escape due to three different mechanisms [13]:

- **Classical losses:** the fast ion is in a non-confined orbit that ends up impacting the walls. A variety of subtypes exist. Prompt losses, produced when a neutral injected by a NBI is ionized in a position where its new orbit will collide with any wall. Ripple trapping diffuse y stochastic toroidal ripple, where fast ions can pass from a confined orbit to a non-confined one due to the loss of homogeneity of the magnetic field due to the magnetic coils being finite elements. .

- **Coulomb collisions:** collisions with electron or other ions produce the thermalization of the fast ions but also change its pitch angle. Therefore the new trajectory of the fast ion may end in a wall. As this particles are quite fast several laps can occur toroidal and poloidally before the impact takes place.

- **Magnetohydrodinamic**: instabilities are fairly common in plasma, they can last in a range from micro to miliseconds. If that instability happens in the same region of a fast ion, its orbit may be altered resulting in the loss of that fast ion. One of the current goals in magnetic confinement research is being able to predict and prevent MHD instabilities in real time because this instabilities can provoke the shutdown of the reaction due to the plasma touching the walls.

2 The Fast Ion Loss Detector (FILD)

FILD is an acronym for Fast Ions Loss Detector. The importance of fast ions inside a Tokamak was already explained in section 1.6. A good understanding of how many of those highly energetic ions are lost is enforced, this is the the reason of the existence of this detector. A 3D render of FIlD's head is shown in figure 2.1.

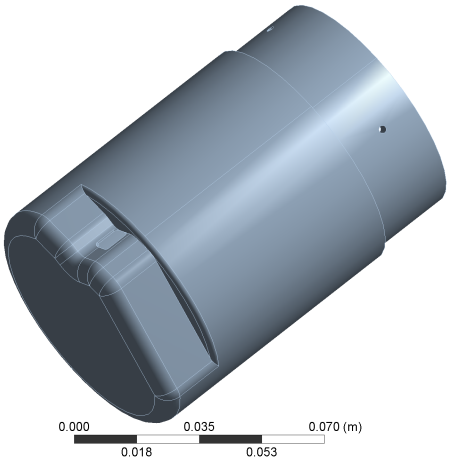

Figure 2.1 FILD head 3D render.

A good FILD must have the following characteristics extracted from Rodríguez thesis [13]:

- Type of suprathermic particle detected.
- Spacial location of losses over the first wall of the reactor.
- Angular distribution of the fast ions. This gives information about the nature of the orbits followed by the ions.
- Good energy resolution to detect the suprathermic particle energy range (from keV to MeV).

- Good time resolution to follow the evolution and frequency of losses due to MHD instabilities.
- Particle flux that impacts the vessel.
- Detector must be flexible and resistant to stand a hostile environment with high neutron flux, gamma rays and high temperatures.

FILD is a scintillator based detector. This means particles, fast ions in this case, collide with a sensible sheet, called scintillator, that registers the impact. Concretely in FILD, fast ions go through a pinhole (figure 2.2) where a collimator is set to prevent the entry of thermal ions. Inside the device, the collision takes place with the scintillator who registers the location of the collision, this data will be necessary to reconstruct the trajectory of the fleeing ion. The scintillator is formed by a sheet of stainless steel that serves as the base for a covering of phosphorus.

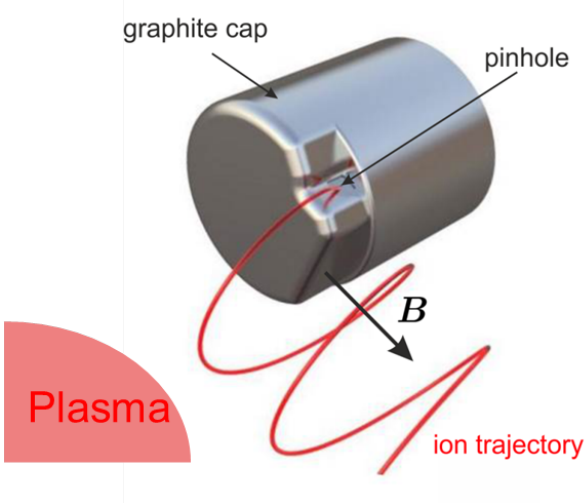

Figure 2.2 Fast ion entering through FILD pinhole [14].

Once fast ions collide with the scintillator, light is emited. This light is collected by an optic system which divides it in two equal beams. One is then received by a high spatial resolution camera (CCD camera) and the other by a high temporal resolution one (APD camera). This leads to a good definition of the escaping ions [15]. This layout is represented by figure 2.3.

Inside ASDEX Upgrade a total of five FILDs are installed, following the distribution of figure 2.4. FILD 1 and 2 are aligned are at the same poloidal position but in different toroidal locations. FILD 3 and 5 are close to the upper and lower divertor respectively. FILD 4 is able to perform fast movements thanks to a Magnetically Driven Reciprocation System (MDRS). FILD 5 is situated between two magnetic coils which facilitates the study of the effect of those coils on the fast ions [16]. FILD measuring positions are a compromise solution between getting good readings and not receiving high heat loads.

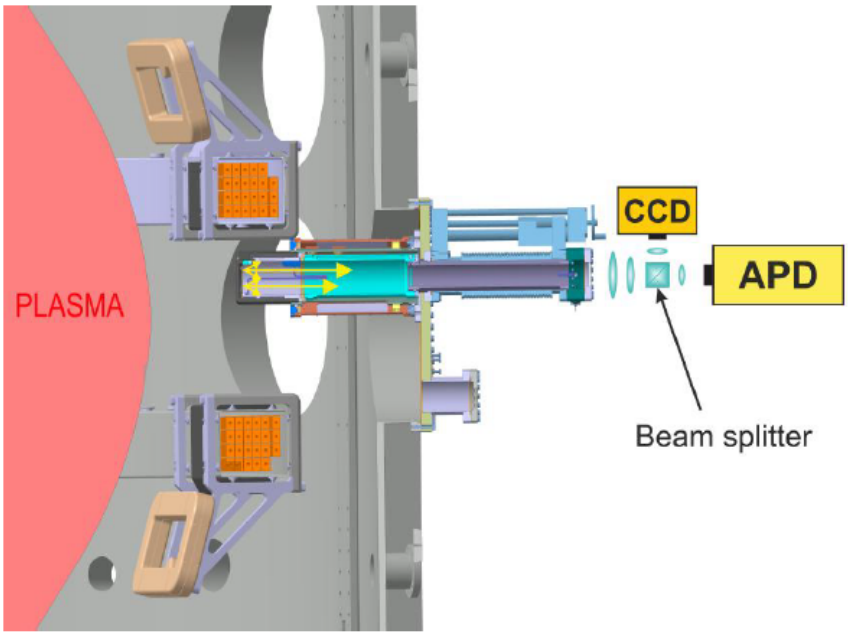

Figure 2.3 Basic layout of the optical collecting system of FILD in MAST-U Tokamak. Light emitted by the scintillator is divided and then received by a CCD camera and a APD camera. [15].

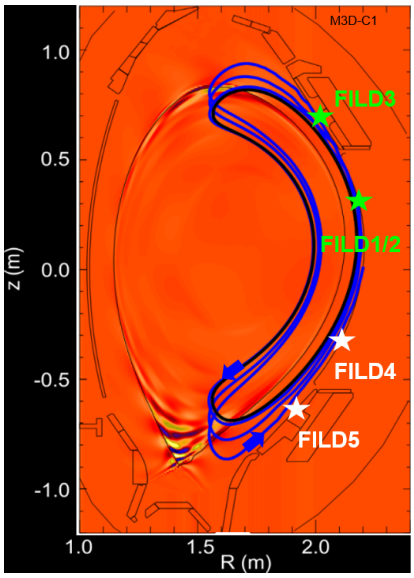

Figure 2.4 Poloidal distribution of FILDs in ASDEX Upgrade [16].

In section 1.4 axisymmetry was presented as one of the pros of the Tokamak design. Meanwhile this is true as a first approximation, if the calculation is more accurate the non-uniformities in the magnetic field produced by discrete magnets (also discussed in section 1.4) disrupt the assumption. Therefore having FILD 1 and 2 in the same toroidal line allows studying its differences which is a measurement of the strength of the axisymmetryc hypothesis. And with a poloidal plane covered thanks to the rest of FILD a good enough idea of the 3D behavior of fast ions along the Tokamak can be obtained.

FILD head is manufactured in graphite and coated with tungsten, a heat resistant material

but not enough for plasma edge temperatures and the ion flux. This is why the head is not always exposed to plasma. Normally the device is in a parking position behind the first wall where it still receives thermal loads but in a bearable levels. When it is time to get some readings FILD head is introduced in the vacuum vessel where it starts collecting fast ions and with them high loads are deposited over the head surface. This situation can't be sustained too long without structural damages. Therefore a good thermomechanical simulation of FILD during its working time must be achieved in order to get FILD working optimally and without damages, this is the motivation of this study.

3 Modeling the particle collisions with FILD

In this section the motion of fast ions and electrons will be simulated together with their collisions with FILD head. To get whether an intersection happens or not, Möller-Trumbore ray-triangle algorithm will be used which will require a previous refinement of the given FILD mesh to get well-defined results. This section corresponds with the core of this work, creating a series of tools that permits this simulations to be flexible and efficient. MatLab software will be used for this chapter.

3.1 Mesh refinement

A 3D model of ASDEX Upgrade vacuum vessel and of FILD head has been provided by CNA (Centro Nacional de Aceleradores) of University of Seville.

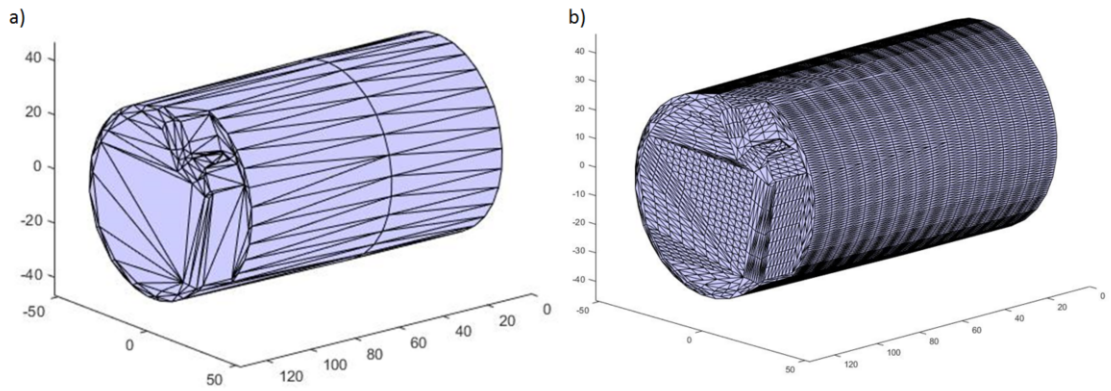

Figure 3.1 FILD head mesh: a) initially b) after triangulation with triangle surface minor than 10 cm^2.

Head model was given as shown in figure 3.1 a). Its geometry is quite simple, a big

cylinder with some flat surfaces, so the mesh can be defined by triangles of a considerable size. This rough geometry would give inaccurate results on which zones of the FILD head receive collisions and therefore heat flux. To solve this, the initial triangles must be subdivided into smaller ones until all triangles get small enough to achieve the desired precision.

For this matter a MatLab program was created. A maximum area is given to the program as an input, then all triangles are checked if their surface is bigger than the reference. If this happens those triangles are subdivided into four equal-area smaller ones, this continues in a loop until no triangle is larger than the reference, at the end with a reference of 10 mm^2 the result is shown in figure 3.1 b). To make this subdivision code from MathWorks repository was used, concretely *subdivide_ tri.m* [17].

3.2 Field Line Tracer

Not the whole exposed surface of FILD head receives impact of particles. Part of those particles collide first with other elements of the reactor. This phenomenon is called *shadowing* [18]. Taking into account that FILD surface is triangulated gives birth to two different types of triangles: plasma wet triangles, which receive collisions of particles and dry triangles, which receive no collisions. This creates zones with a higher heat flux than the bordering ones with the consequent thermal stress.

In section 1.3 full orbit motion was described. Applying this in MatLab suppose a high load in terms of computational resources. For this tool, particle motion will be simulated as if they were following the magnetic field lines on the plasma. This reduces code complexity and computational time and doesn't harm the final goal, that is developing a tool to obtain the heat flux map over FILD in numerous situations, not a precise simulation of plasma particles.

Therefore a magnetic field line tracer must be developed in order to register which triangles are wet or dry. The most straight forward approach to this problem is initiate n particles in random positions in plasma and after some simulation time see how many have collide or not. This obviously is not a really good idea, as the size of n should be big enough to assure that every possible trajectory is followed. So the contrary approach results as an easier path. Particles will start in each triangle (defined by its center of masses) and will go "back in time" until it collides with the reactor walls or other detector or a given time passes uneventfully.

If time passes and no collision is registered then that trajectory would be feasible and therefore that triangle would be wet. Otherwise, if a collision takes place, that trajectory could not take place so the triangle would be dry. For this collisions, particles going through the positive and negative direction of the magnetic field will be registered.

Particle trajectories are also subjected to the magnet and plasma configuration in the moment of the simulation. This magnetic field data has been obtained from ASDEX Upgrade inner database of plasma shots, where for a given shot and time a magnetic field

3D mesh is provided.

Having the magnetic field mesh the particle motion simulation can start. The simulation starts in a node of FILD head, in given *x y z* position at time t_0. As the particle will follow magnetic field lines, the objective is to define the magnetic field in its position and use that vector as its velocity to calculate its position in the next instant. Integrating this way results in a complete trajectory in the integration interval.

First, particle parameters in the given position are calculated:

$$\alpha = tan^{-1}(y/x) \tag{3.1}$$

$$Radio = \sqrt{x^2 + y^2} \tag{3.2}$$

With this parameters magnetic field vector in particle position can be obtained by interpolating the 3D mesh, for this, *Radio* is used. The result is in cylindrical coordinates and to convert it to Cartesian, a rotation matrix is used:

$$\begin{bmatrix} B_x \\ B_y \\ B_z \end{bmatrix} = \begin{bmatrix} B_{radial} \\ B_{toroidal} \\ B_z \end{bmatrix} * \begin{bmatrix} cos(\alpha) & sin(\alpha) & 0 \\ -sin(\alpha) & cos(\alpha) & 0 \\ 0 & 0 & 1 \end{bmatrix} \tag{3.3}$$

With the magnetic field vector defined in the particle position, integration can start and the whole trajectory recorded. Those trajectories are expected to be closed ones as those particles must be confined within the reactor. Once the collision check is run it will be seen which ones lose this confinement due to this collisions with the 3D structures of the reactor.

3.3 Triangle-Ray Intersection

Once all trajectories for a given FILD at a given measuring position are recorded, it is time to check if any collision occurs before the integration time is due. This is done by checking every segment of a particle trajectory with all the triangles that form the vacuum vessel and the five FILDs. A highly vectorized MatLab code of Möller and Trumbore [19] intersection algorithm is used. This MatLab version was obtained from the MathWorks repository, the function is called *"TriangleRayIntersection.m"* [20].

The algorithm uses an unitary triangle perpendicular to the x=0 plane and expressed in barycentric coordinates. In barycentric coordinates, points inside a triangle are written as T = f(u,v,w) with each of those coordinates being equal to 1 in a vertex a 0 in the other two. This creates a contour condition inside the triangle (eq. 3.4) that converts the triangle from

3D to 2D. An equilateral triangle in barycentrial coordinates is represented in figure 3.2.

$$u+v+w=1 \tag{3.4}$$

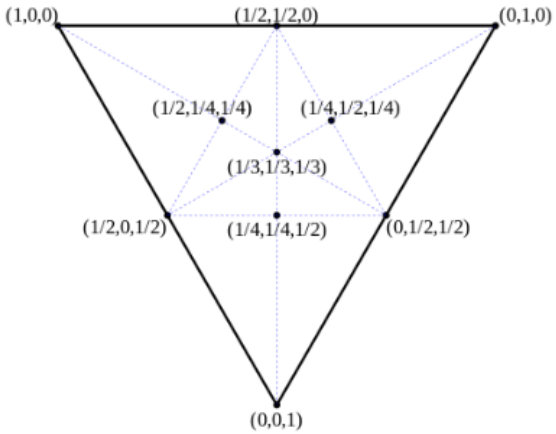

Figure 3.2 Equilateral triangle expressed in barycentrical coordiantes [21].

In this coordinate system a point within the triangle is defined by:

$$\begin{cases} T(u,v) = (1-u-v)*V_0 + u*V_1 + v*V_2 \\ u \geq 0 \quad v \geq 0 \quad \text{eq. } 3.4 \rightarrow u+v \leq 1 \end{cases} \tag{3.5}$$

Being $V_{0\,,\,1\,,\,2}$ the vertices of the triangle.

A ray is then define as equation 3.6, passing by the origin and with normalized direction D.

$$R(t) = 0 + t*D \tag{3.6}$$

The intersection point (if there were one) will be the equality between equations 3.5 and 3.6:

$$\begin{aligned} 0+t*D = (1-u-v)*V_0 + u*V_1 + v*V_2 \rightarrow \begin{bmatrix} -D & V_1-V_0 & V_2-V_0 \end{bmatrix} * \begin{bmatrix} t \\ u \\ v \end{bmatrix} = 0-V_0 \rightarrow \\ \rightarrow M * \begin{bmatrix} t \\ u \\ v \end{bmatrix} = 0-V_0 \end{aligned} \tag{3.7}$$

So the coordinates from the intersection point (u,v) as well as the normalized distance

from the origin (t) are both the results of linear equations with the light computational load this means.

For any triangle in a 3D environment it will have to be first converted. This is done by translating it to the origin and then by multiplying it by the inverse of the transformation matrix M, from equation 3.7. This process is summarized in figure 3.3.

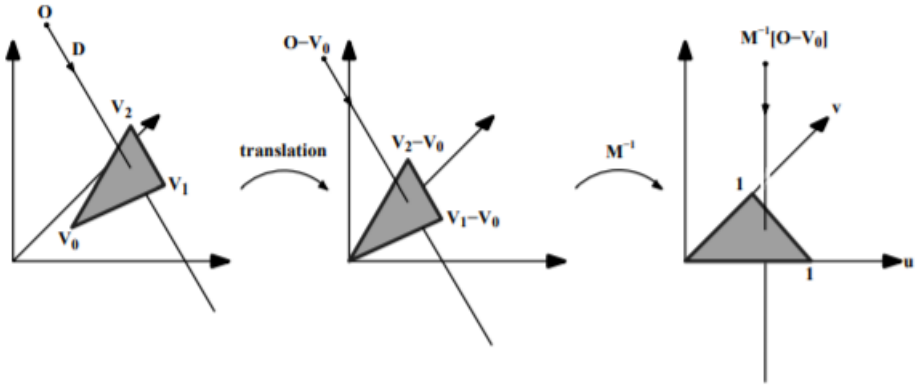

Figure 3.3 Steps to follow from a 3D triangle to a Möller-Trumbore-ready triangle [19].

For further information about the algorithm or its general application refer to the original paper [19].

This algorithm is applied to every segment of each particle trajectory. During the checks if one segment registers an intersection with any triangle of the environment, the function for that trajectory stops and the origin of that trajectory is recorded as a wet one and so on the triangle it represents.

With this algorithm together with the field line tracer the triangles that form FILD head are already defined as wet or dry. For the wet ones its position and angle of incidence is recorded as they will be necessary in the upcoming sections. Being this angle of incidence, the angle between the field line and the normal to the surface.

3.4 Optimizing the code

In some scenarios where FILD head is highly exposed, simulation time can takes even days for a well refined mesh. Getting down this time, saving computational resources, is essential in order to make the code more user friendly and useful. In this section the optimization methods used are presented.

3.4.1 OcTree

Vessel render (figure 3.4 alone accounts for 162000 triangles and still it would have to be added up the amount of faces in each of the five FILDs. This means that each segment of

all trajectories would have to check for collision over 162000 times, this is computationally unacceptable. OcTree algorithm has been used to cut down this computational load to more acceptable levels. This algorithm has already been used in other studies with similar profiles as [18].

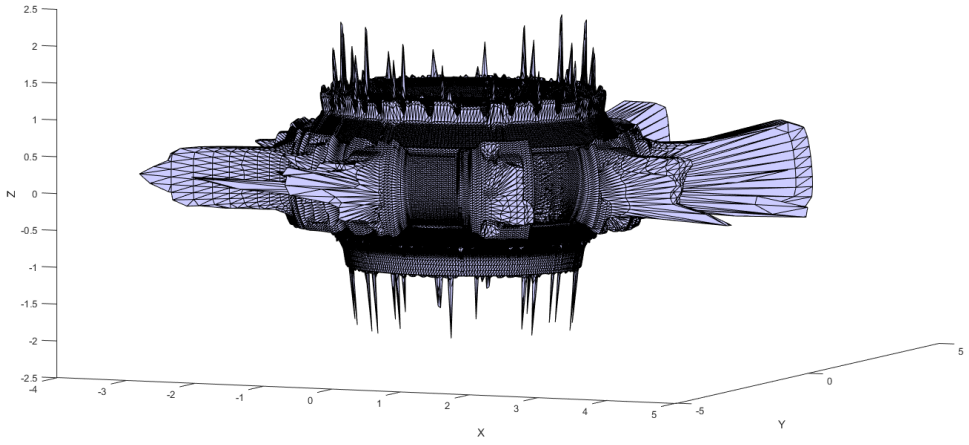

Figure 3.4 Vessel mesh used for MatLab simulations. Peaks represent ports for detector or other devices.

OcTree intends to decrease total computational time by reducing the amount of triangles each segment has to be compared with. The algorithm divides the to-be-compared-with mesh into two submeshes (called *bins*) with the same amount of points, this process is repeated with each new smaller mesh until a certain criteria is found (by default, the amount of points inside a bin is equal or smaller than a tenth of the total amount). Now the intersection would only be checked with points inside the same bin as the segment, reducing drastically the computational time.

The problem is that the triangle-ray intersection does not check with points but with triangles. So as the triangle is not completely defined it won't be checked with the segment in question. This idea is illustrated in figure 3.5.

To solve this, an index relating each vertex with the face it belongs has been created. This index has the same length as the amount of points in the mesh, in each row the faces where this vertex is participating are stored. This means that for the points contained in target bin, this index returns all faces related to said bin. These faces will be then checked with the ray-triangle intersector.

Also the situation were the initial point of the segment and the final one are not in the same bin must be covered. In this case it may happen that segment passes by a third bin. This could be solved by giving the field line a very small step but this will result in an increasing of the computational time. A faster solution is to not use the OcTree algorithm in this particular case were initial and final points of the segment are in different bins.

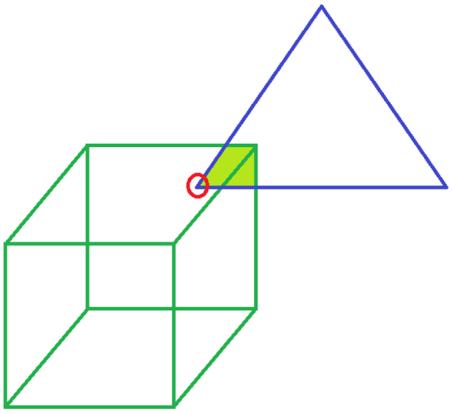

Figure 3.5 The green colored zone of the bin won't be checked if only full triangles inside the bin are taken into account.

The efficiency of the algorithm depends on the configuration of the simulation. Generally a configuration that would increase the computational time, will also increase the effect of OcTree. For instance, if FILD is parked all the trajectories will collide almost at the beginning of the simulation, so the algorithm won't be called as many times as if the head was totally exposed and, due to this, most of its triangles were wet.

So there is no way to give an accurate number of the impact of this algorithm in the overall computational time. However, a demonstration case has been prepared to illustrate the benefits of using the aforementioned algorithm. For this example a medium refined mesh was used with a total of 747 faces. Simulations were run for each FILD in three positions: at parking position and at 4, 8 cm of insertion. Results are shown in table 3.1. Plasma shot used was ASDEX Upgrade #34570.

Table 3.1 Comparison between using or not the OcTree algorithm in a medium refined mesh at three different positions for all FILDs. ASDEX Upgrade shot #34570 was used.

	FILD 1			**FILD 2**			**FILD 3**		
Insertion [m]	0	0.04	0.08	0	0.04	0.08	0	0.04	0.08
OcTree [s]	623.33	1690.4	2240.2	855.61	745.93	633.85	1477.7	1070.9	1350.3
no OcTree [s]	739.48	2339.6	3009.9	811.53	820.3	731.28	2052.3	1217.1	1739.4
Savings [%]	15.707	27.748	25.572	-5.432	9.066	13.323	27.998	12.012	22.370
	FILD 4			**FILD 5**					
Insertion [m]	0	0.04	0.08	0	0.04	0.08			
OcTree [s]	916.17	1368.4	1589	1593.8	1727.7	1983.4			
no OcTree [s]	1162.3	1850.1	2249.3	1949.2	1859.1	2194.1			
Savings [%]	21.176	26.036	29.356	18.233	7.068	9.603			

Even though as it was stated before no real percentage of saved time can be defined, a similar value can be obtained with the mean of the results as those simulations cover a wide range of situations. Therefore applying the OcTree algorithm results in a mean saved

time of 17.32%.

FILD 2 is the only one where in a due position (concretely parking) using OcTree means increasing the computational time, from 811.53 seconds to 855.61 , 5% higher. FILD 2 has the singularity of staying dry through all simulations even at 12 cm insertion, due to being severely caged between other elements of the vacuum vessel. So all its positions are similar to a normal parking where intersections occur almost immediately. This was pointed as one of the cases where OcTree efficiency would be harmed. On the other hand FILD 4 presents the biggest impact by the algorithm, with a peak saved time of 29.36%. This was also expected as FILD 4 has the biggest count of wet triangles of all five FILDs and it is in wet triangles were OcTree shines due to a bigger number of iterations of the triangle-ray intersection algorithm.

Other FILDs don't take advantage of the algorithm in the same way as they peak at different insertions instead of at the largest one. The reason behind this may be that the interior of the vacuum vessel is not completely uniform and can project unexpected shadows. Another possible reason is that several simulations were run in parallel what might have drained resources from one simulation to another, this reason is improbable as CPU usage was normally around 40%.

3.4.2 Frontier analysis

A frontier can be drawn between the wet and dry zones. If this frontier were found, it would be known which triangles were dry and therefore no field line intersection check would be needed.

To find this frontier a rougher mesh has been used, concretely one with a maximum triangle surface of 47 mm^2 and 747 faces. Field line tracer is run for the whole set of triangles giving the results shown in figure 3.6. For this example FILD 4 with 2 cm of insertion will be analyzed.

FILD is then moved to a local coordinate system where it is aligned with one axis. X'-axis has been chosen for this subject as shown in figure 3.7. The wet triangle with the highest X' value and the dry one with the lowest are then found, from them the furthest and nearest vertex are then saved. Those vertices define two planes perpendicular to the X' axis that encapsulate the frontier. A security margin of 0.02 m has been added to both limits.

Now the target mesh, a enough refined one, can be used. This new mesh has to be also expressed in the local coordinate system. Triangles whose barycentric has a X' value lower than the frontier will be wet and no intersection check will be needed, trajectory has to still be calculated as the intersection angle is required for the thermal analysis. If the X' value is higher, triangle will be dry and no further calculation will be necessary. In the halfway case where $X'_{min,\,front} < X' < X'_{max,front}$, trajectory will be calculated and intersection checks made as there is no certainty whether those are wet or dry triangles. Trajectories and intersection checks must be made in the global coordinate system. Results from this second simulation with the target mesh are shown in figure 3.8 for this example case.

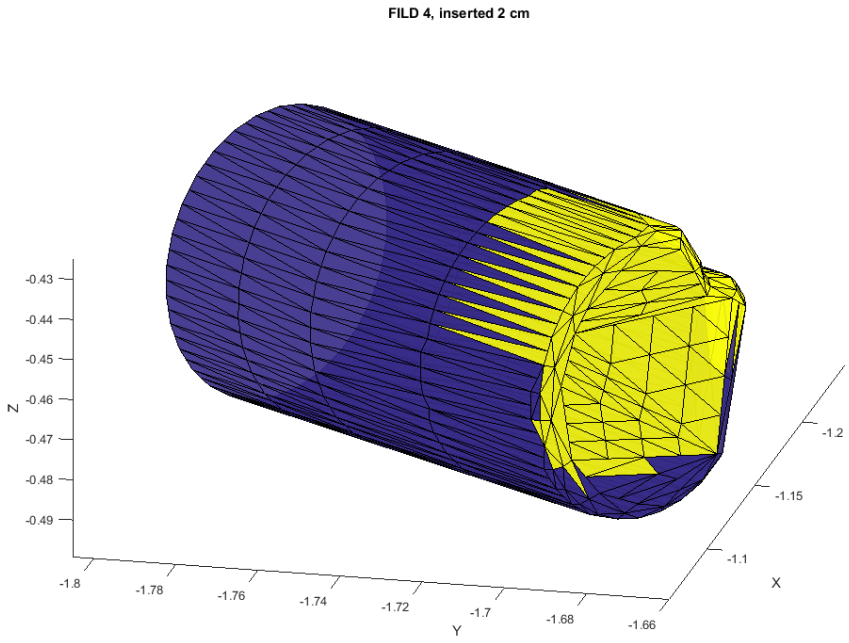

Figure 3.6 Auxiliary mesh checked in order to get the frontier. FILD 4 with 2 cm of insertion was used. Yellow triangles represent wet areas and blue triangles, dry ones.

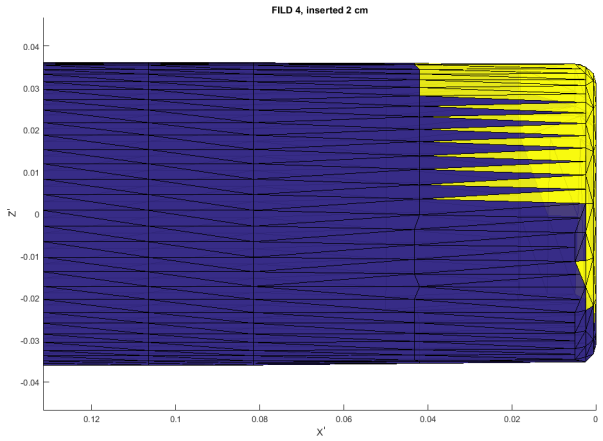

Figure 3.7 Auxiliary mesh in local coordinates. Maximum wet point and minimum dry point are collected in order to aim the next well refined analysis in that area. A security margin of 0.02 m has been added to both sides.

Experimentally it has been observed that $X'_{min,\,front}$ tend to be near X' = 0. This is due to the particular geometry around the pinhole where is easy that one of its triangles stays dry. So generally speaking calculating or not the minimum of the frontier tends to have little impact. Nevertheless this calculation has been kept in the code as it would be greatly beneficial when $X'_{min,\,front} > 0$ and be negligible in the opposite case.

Generally, computational time saved by this addition is way bigger than the consumption of searching the frontier. Initial mesh has to be refined enough to give a general idea of the position of the frontier, if this initial mesh was too rough results would be faster but

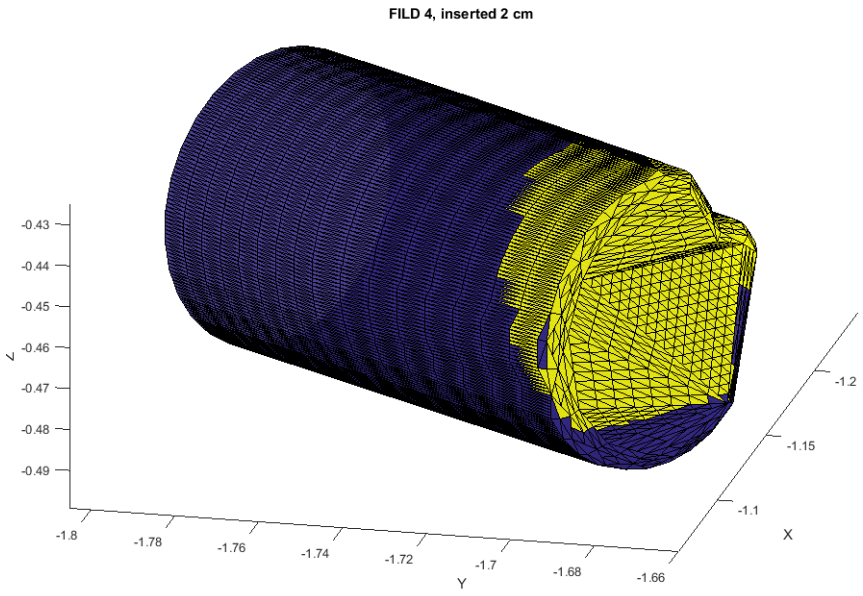

Figure 3.8 End results for FILD 4 with 2 cm insertion. Using a mesh with 8958 faces versus the 747 faces of the auxiliary mesh. Yellow represents wet triangles and blue dry ones.

useless.

Saved time increases with the refine level of the objective mesh as more iterations are not needed and therefore the weight of searching for the frontier will be negligible.

As a secondary improvement over the no frontier case, a new condition has been added. In the no frontier scenario, collisions had to be checked to all five FILDs in addition to the vessel. But if any of those FILDs is in parking position, it is certain that the field line won't impact with that FILD, therefore there's no necessity of checking them. This means a lower computational time specially for cases with a severely refined mesh.

Table 3.2 Comparison between using or not the frontier algorithm in addition to OcTree in a highly refined mesh at three different positions for all FILDs. ASDEX Upgrade shot 34570 was used..

	FILD 1			**FILD 2**			**FILD 3**		
Insertion [m]	0	0.04	0.08	0	0.04	0.08	0	0.04	0.08
OT+front [s]	694.92	1404.3	2126.3	499.75	451.68	436.56	1124.9	9955.6	12595
OT+no front [s]	7200	14501	24525	7851.3	7552.1	7453.4	1377.5	9984.1	13359
Savings [%]	90.348	90.316	91.330	93.635	94.019	94.143	18.338	0.285	5.719
	FILD 4			**FILD 5**					
Insertion [m]	0	0.04	0.08	0	0.04	0.08			
OT+front [s]	3742.1	10453	18262	11237	16878	24353			
OT+no front [s]	7413.6	12742	18358	12828	17173	23435			
Savings [%]	49.524	17.964	0.523	12.403	1.718	-3.917			

A new set of simulations were run in a similar way to the previous section. Simulations have been run for all five FILDs at three different insertions (0, 4 and 8 cm) and in two ways, only with OcTree and with OcTree and frontier algorithm. Results are shown in table 3.2. Savings produced by this additions show two very differentiated groups: FILDs 1 and 2 and FILDs 3, 4 and 5. First group see an improvement of 92.29% in average meanwhile the second one of only 11.40%. This differentiation comes from the position of those groups, as it was already shown in figure 2.4, FILDs 1 and 2 are located approximately in the mid plane and the second group is positioned closer to the upper and lower divertors. This means that for FILDs 1 and 2 the frontier will have a more perpendicular profile to the FILD axis than for FILDs 3, 4 and 5 (the inclined profile of this second group is easily seen in figure 3.8), therefore the frontier will be much wider and the benefits of searching for it palliated. Also this differentiation can also be produced by the presence of limiters near the FILDs, limiters are curve structures of the first wall who are tasked with maintaining plasma shape; this limiters can produce the shadowing of the FILDs near them (3.9). Those effects peak at FILD 5 with 8 cm of insertion where applying the frontier analysis becomes counter-productive.

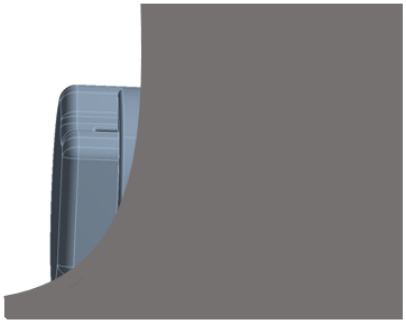

Figure 3.9 Schematic of a limiter shadowing a FILD. A similar situation to this figure happens to FILD 4.

In average searching for this frontier means saving up 43.76% of computational time. And in total, using OcTree algorithm, locating the frontier and only checking collisions with non-parked FILDs mean a total average saved time of 53.50%.

4 Thermal Model for plasma facing components

In this section the cosine thermal model for plasma facing components will be introduced and justified. As well as the process required to implement it. Also a brief overview of the total software developed is included.

4.1 Cosine model

The thermal model used for this work is the so called cosine model. This model has been widely used in different thermal analysis of PFC (Plasma Facing Components) [18], [22], [23], [24]. Cosine model (eq. 4.1) is a convective model due to convection being the predominant heat source for plasma facing components [23] as FILD. It allows to estimate the heat flux parallel to the magnetic field lines ($q_{||}$) as a function of experimental parameters q_0 and λ_q. Only in points were plasma itself collides this model cannot be used, as FILDs are separated enough from the separatrix (the frontier between confined plasma closed magnetic field lines, and open ones) this study will use the aforementioned model.

$$q_{||} = q_0 * e^{-\frac{\delta}{\lambda_q}} \tag{4.1}$$

The heat flux, due to its convective origin, is the result of the collision of particles with surfaces. Therefore particle flux (Φ) have an equivalent representation as the heat flux (eq. 4.1) [25]:

$$\begin{aligned} \phi \ \alpha \ \phi_{||} * cos(\alpha) \\ q \ \alpha \ q_{||} * cos(\alpha) \end{aligned} \tag{4.2}$$

This model only accounts for the deposition of power parallel to the magnetic field lines. Again Mitteua [23] takes this approximation as valid if the objective surface is not large.

Stangeby [26] relates the perpendicular and parallel influx of particles as a way of checking the availability of this model for certain situations:

$$\frac{\phi_{\perp}}{\phi_{||}} = \sqrt{L_f/L} \tag{4.3}$$

Being L_f, the length front face and L = π*R_{FILD}

$$\frac{\phi_{\perp}}{\phi_{||}} = \sqrt{0.1/(\pi * 1.6)} \rightarrow \phi_{||} \gg \phi_{\perp} \tag{4.4}$$

Now that the feasibility of cosine model for this study has been proven, equation 4.1 can be dissected:

- q_0: upstream peak heat flux, is the heat in the separatrix. Sieglin [22] and Mitteau [23] gives it a value of around 100 MW/m^2.
- δ: distance of the target from the separatrix. $\delta = s - s_0$.
- λ_q: e-folding length of the heat flux.

Experimentally the power that escapes convectively the reactor to impact with the first wall is known, via power balance [22]. Knowing this power and the total surface, q_0 is obtained by imposing that this power is equal to the received by all wet surfaces.

The cosine model is a experimental model based in the knowledge that the convective parallel heat is the predominant and that is evolves as an exponential. The λ_q parameter is not well known yet and therefore a range of parameters has to be studied in order to find one that adjusts to reality. Different studies [18], [23],[27] situates the range of values of λ_q from 1 mm to 1 cm.

Equation 4.1 is defined in the outside mid plane (omp) as the results varies poloidally. This change can be input directly by calculating the heat flux as a function of $\rho_{poloidal}$ (this concept will be defined in next section) or by adding an new parameter f_x. The first case will be the used for this study.

Even though heat flux will be calculated as a function of $\rho_{poloidal}$, f_x parameter is explained below as the physical idea of the difference between omp and other planes is better explained using this parameter. As it was previously stated the convective model follows the magnetic field lines, therefore if the density of field lines decrease the rate of variation of the heat flux will be slower. This is what happens when moving polloidally to the divertors, magnetic field lines will open gradually as represented in figure 4.1 a). This is accounted by the

magnetic flux expansion ($f_{x,\,mag}$).

$$f_{x,mag} = \frac{R_{mp} * B_{pol}^{mp}}{R_x * B_{pol}^{x}} \tag{4.5}$$

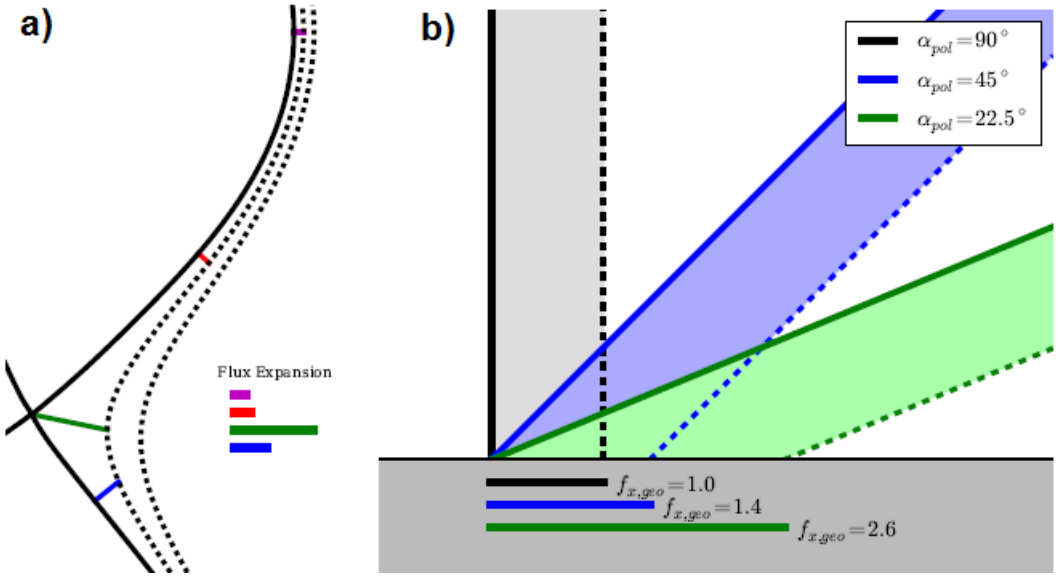

Figure 4.1 a) Magnetic flux expansion near the divertor b) Geometric flux expansion [22].

Also the same effect can take place with the incidence angle between field lines and surfaces. This is illustrated in figure 4.1 b). This variation is represented with $f_{x,\,geo}$. This geometric effect can also be account separately by multiplying q_0 by the cosine of the angle between the normal surface and the magnetic field line. This idea was already presented in equation 4.2.

$$f_{x,geo} = \frac{1}{sin(\alpha_{pol})} \tag{4.6}$$

Knowing that $f_x = f_{x,mag} * f_{x,geo}$, the flux expansion is integrated in the cosine model is represented in equation:

$$q_{||} = q_0 * e^{-\frac{\delta}{\lambda_q * f_x}} \tag{4.7}$$

4.2 Model application

This model will be applied using the MatLab software. As it was stated in the previous section, the magnetic flux expansion won't be explicitly represented. The magnetic effect

will be taken into account by transforming equation 4.1 from coordinate δ to $\rho_{poloidal}$. Meanwhile the geometric part will be calculated with the pitch angle between field line and wet surface. As this model requires the impact between magnetic field lines and FILD faces, only wet triangles will receive it.

First the poloidal normalized radius (ρ_{pol}) must be defined. This normalized radius has its zero value at the magnetic axis of the plasma and is equal to the unit at the separatrix. As the separatrix real position varies in the z-axis, $\rho_{pol} = 1$ will change its Cartesian position. This variation is equivalent to the shown by the magnetic flux expansion.

For this task kk library from ASDEX Upgrade has been used. kkMap function transforms a point from Cartesian coordinates to poloidal ones for a given plasma shot. With this function the position of the separatrix (s_0) can be obtained by imposing $\rho_{pol} = 1$. Therefore equation 4.1 is already defined in the omp.

To get the rest of points the normalized position of all FILDs must be obtained. Again the kkMap function is used, this time with all wet points of the FILD heads. Power deposition over FILD will come from the interpolation between the heat flux value at $\rho_{pol,\,omp}$ at $\rho_{pol,FILD}$.

Finally the geometric flux expansion is applied by multiplying the previous result by the cosine of the pitch angle that was already calculated in section 3.3.

By this point the heat flux [W/m^2] in each wet triangle is already known, so by multiplying each one by its own surface the total power received by the FILD head at that position is known.

4.3 Numerical tool description

Now that the whole simulation is finished and results ready to use in ANSYS has been obtained, an overview of the inner operation of the software is given as a user-friendly fast way of getting into its usage.

First inputs are defined, the only output is the heat flux through each of the triangles that form FILD:

- FILD mesh.
- Refinement for the auxiliary and target FILD meshes.
- Vacuum vessel mesh.
- Magnetic field mesh.
- FILD position and target FILD for the simulation.

Figure 4.2 represents the basics of the operation. First, the FILD mesh is refined into

two different steps, an auxiliary mesh to find the frontier between dry and wet triangles and a well refined one that will be the real target of the simulation. Those two meshes together with the vessel mesh are carried into *field_ line_ tracing.m* where a *traject* structure is obtained. Within this structure information of each trajectory is kept as well as if each triangle is dry or wet. *traject* is run in *wet_ triangles.m* where the intersection angle (α) is calculated for each wet triangle. *traject* and $\alpha$are finally used in *q_ map.m* to get the resulting heat flux in each triangle. So until *q_ map.m*, the program would be related to chapter 3 meanwhile the rest would linked with this very chapter.

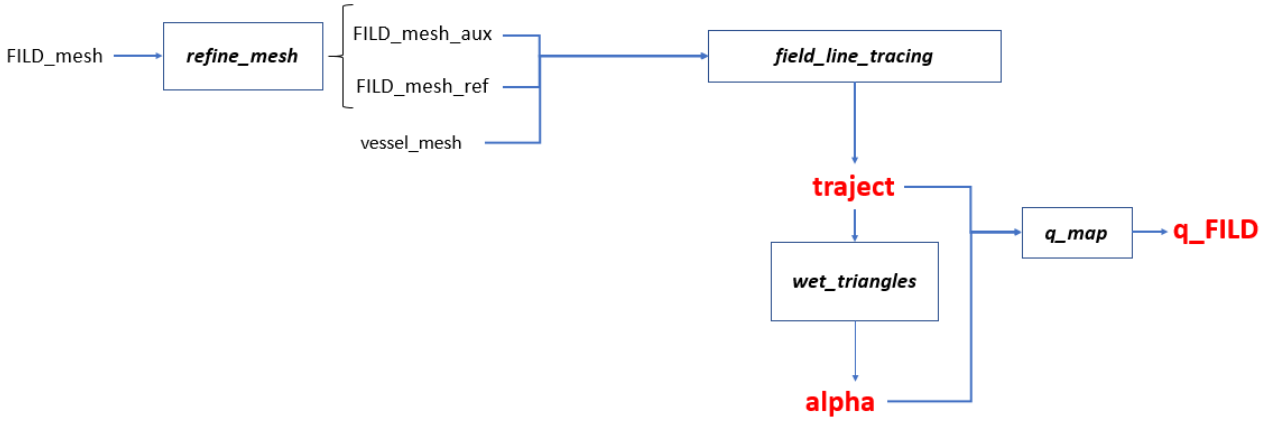

Figure 4.2 Basic overview of the simulation software. In bold are scripts are in red, end results.

As *field_ line_ tracing.m* represents the major part of the software, a more detailed version of its inner operations is shown in figure 4.3.

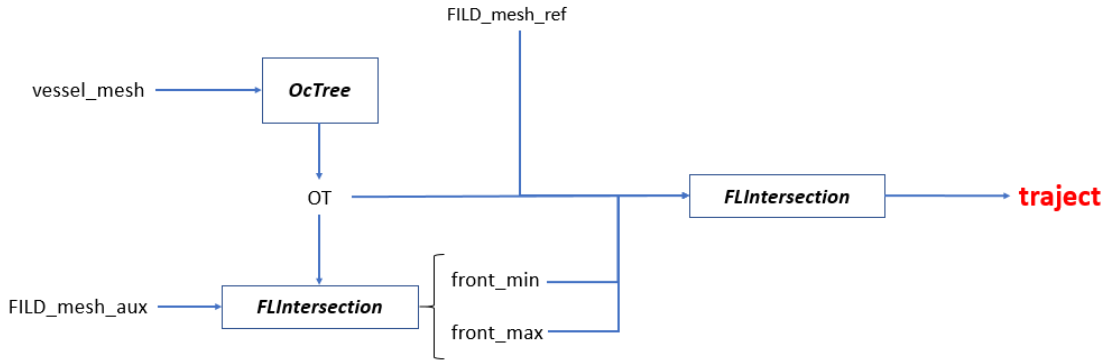

Figure 4.3 Inner operation of *field_ line_ tracing.m* script. Used to get the trajectories born in each triangle and discern whether is dry or wet. Scripts in bold and results in red.

First the OcTree algorithm is applied with the vessel mesh, giving birth to the OT class which contains all the information related with the OcTree bins. This class in conjunction with the auxiliary FILD mesh are used in *FLIntersection.m*, script that checks for collisions, to obtain the limits of the frontier. Again the same script is used but this time to analyze the target mesh between the limits of the frontier. The result is the *traject* structure.

5 Results

In this chapter one specific FILD position is studied in ANSYS software in order to obtain the temperature profile in different scenarios. The aim of this chapter is not to discern whether the FILD will be damaged or not in that situation but to show the potential uses of the results from the numerical tool developed in this work.

The studied case is FILD 4 with an insertion of 3 cm. From MatLab a TXT file is returned, composed by the node ID, XYZ coordinates and heat flux in W/m^2. This data is fed to ANSYS *Transient Thermal* analysis system through the *External Data* component system. FILD mesh used for ANSYS is not the same as the used for MatLab, which was a rougher one, a comparison between both meshes can be found in figure 5.1.

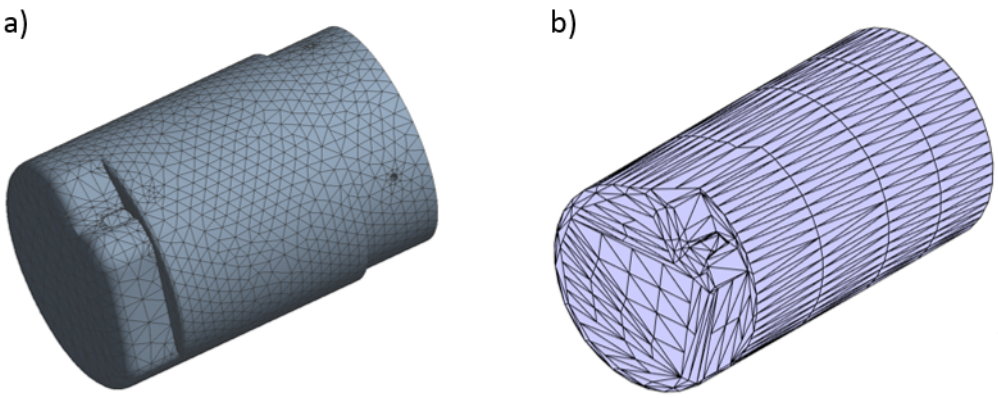

Figure 5.1 a) Mesh used for ANSYS, more detailed to get better end results. b) Mesh used for MatLab, rougher to lower computational time.

ANSYS mesh is more detailed in order to get more accurate results, on the other hand MatLab mesh looks for efficiency and therefore has little details. The highlights in their differences are the pinhole, that is treated as a plane in MatLab and the end part were ANSYS mesh is shorter and more detailed, also in general corners are not as smooth in MatLab as in ANSYS. To transfer the data from MatLab to ANSYS faithfully, surplus

points have been cut out as well as the points in the detailed bottom zone; this is easily justifiable as those points have never gone wet during all done simulations. Pinhole points have not been touched as their influence in the final results are meaningless. Also data from MatLab is not in the same position as in ANSYS this has been corrected via the *Rigid Transformation* field of *External Data*. Numbers used in the correction are shown in figure 5.2

Rigid Transformation		
Origin X	0	m
Origin Y	0	m
Origin Z	-0.196	m
Theta XY	192	degree
Theta YZ	0	radian
Theta ZX	-90	degree

Figure 5.2 Correction to MatLab data done using a rigid transformation throught ANSYS's *External data* component system.

To check if there is a good correlation between MatLab and ANSYS mesh *reverse mapping* utility from ANSYS has been used. From the given mesh ANSYS develops its own triangulation where the software will work by interpolating the heats of the MatLab mesh were located in the barycenter of the triangles composing that mesh. Refinement of ANSYS mesh can be controlled with the *relevance* parameter, in figure 5.3 FILD mesh is shown with relevance of 25 and 100. The similarities between both ANSYS meshes and MatLab one are then checked with reverse mapping, which checks the differences between source and mapped data [28], results are shown in figure 5.4.

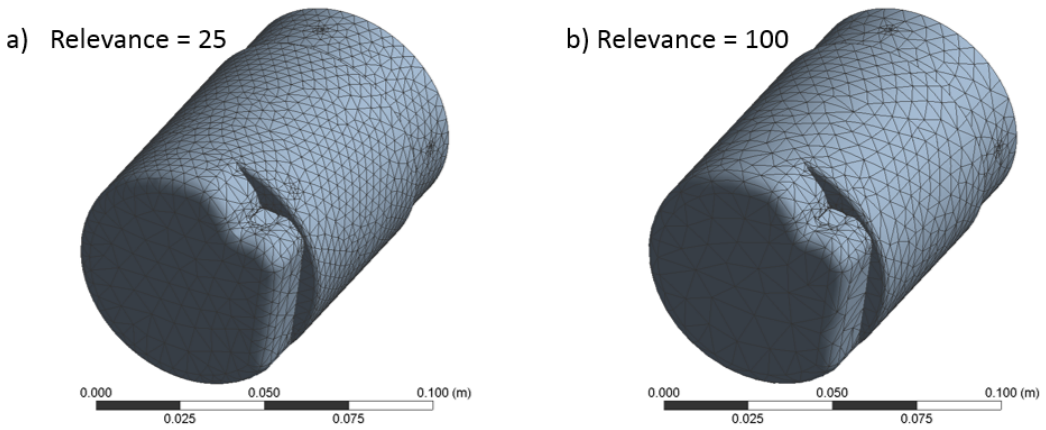

Figure 5.3 ANSYS mesh triangulated with a) relevance = 25; b) relevance = 100.

Results, as expected, are better with a higher relevance being the most conflictive zone around the rounded corner of the front of FILD. In future versions, if needed, a more refined mesh of that conflictive surface can be prepared for MatLab to assure better results

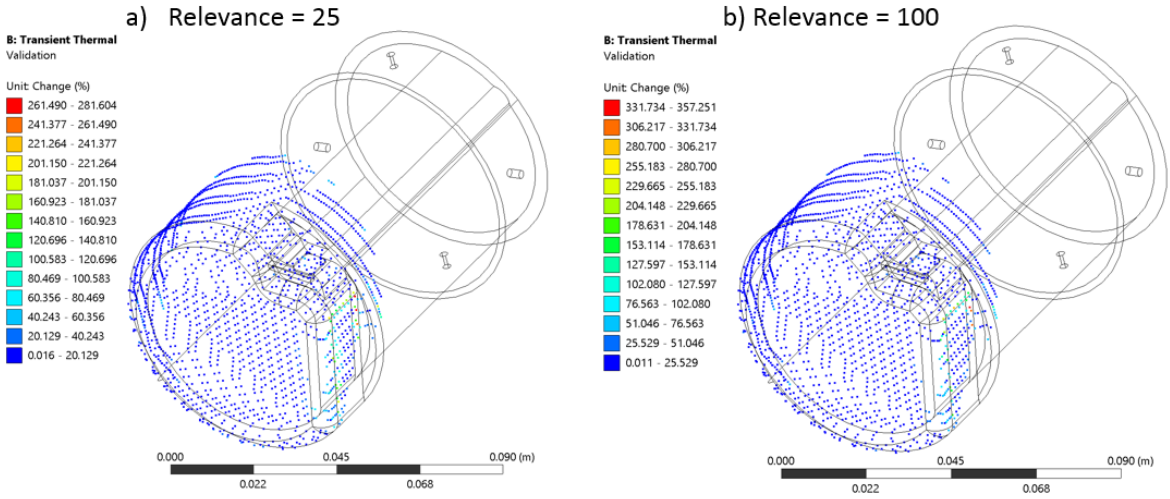

Figure 5.4 Validation results via reverse mapping for a) relevance = 25; b) relevance = 100.

there. Nonetheless that area is not critical for this scenario as the highest thermal flux is located in a well mapped surface as will be shown later. For both situations a simulation with a 20 seconds long exposition has been run, getting the relevance-25 mesh a maximum temperature of 730.74ºC and relevance-100, 732.87ºC; a 0.29% difference that shows the convergence of the mesh. Even though the difference is quite small and relevance-25 mesh could be used, relevance-100 will be the chosen one due to it having slightly better results with no significant time increase.

In figure 5.5 it is shown separately the wet/dry mesh (5.5 a)); the heat map without taking into account the intersection angle α, this is the whole heat flux being totally parallel (5.5 b)) and, finally, the addition of both situations to give birth to the heat distribution for FILD 4 at 3 cm insertion (5.5 c)).

Two scenarios have been prepared for FILD 4. A 20 seconds cyclic simulation and an insertion during another 20 seconds. For both simulations an initial temperature of 100ºC has been chosen as it is common for FILD to stay hot due to a prior operation of the detector and the lack of active cooling. Also a contour condition has been set as 100ºC for the back of FILD in order to dissipate the incoming heat flux.

First scenario represents the normal operation of a FILD. During a plasma shot FILD goes out and into parking position several times to control its temperature. This simulation has 1 second periods of no thermal load which mean the parking position and then another second of full heat load which is the inserted period. It could be discussed whether the duration of the simulation is unrealistic for current plasma shots but in the future ITER this duration may be a reality, also the aim of this section is not to give a realistic simulation of a FILD operation (i.e. there is no transition between parking, 0 cm, and 3 cm insertion) but to present the possibilities this work opens in matter of thermal simulations of FILD.

Results for the first scenario are shown graphically in figure 5.6 where the maximum temperature at the FILD head is represented as a function of time. As it was expected the cyclic and discrete nature of the simulation is translated into sawtoothed graph. The

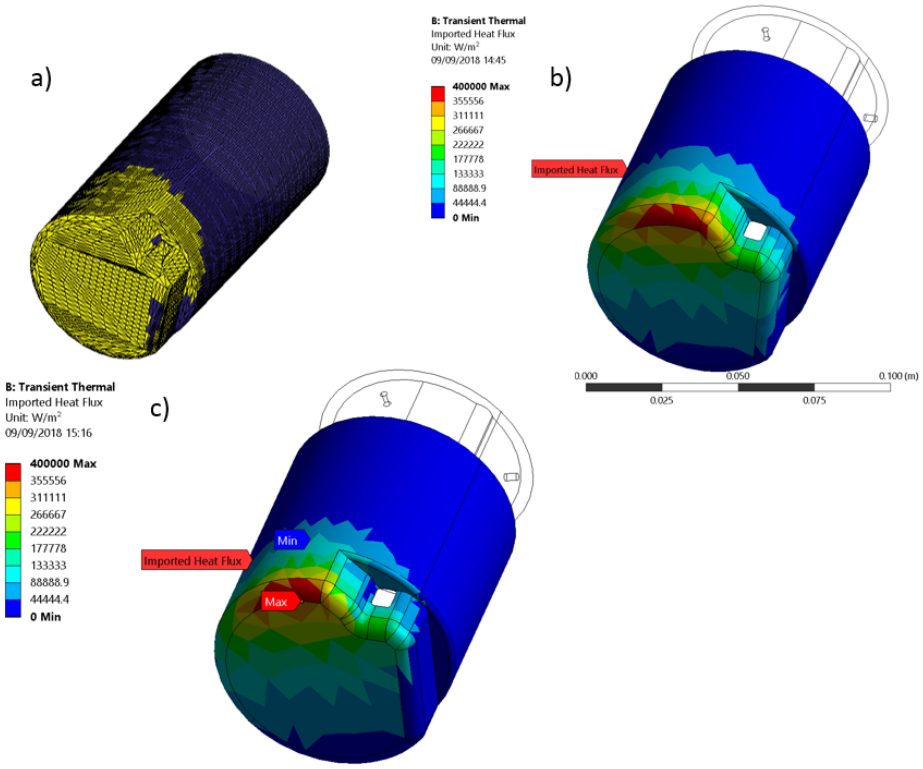

Figure 5.5 For FILD 4 with 3 cm of insertion: a) wet (yellow) or dry (blue) mesh; b) heat flux distribution for totally parallel convective flux and no shadowing; c) heat flux distribution accounting for shadowing and intersection angle of the colliding particles.

three intermediate states represented, help showing the irregular heating of FILD that was already advanced in figure 5.5.

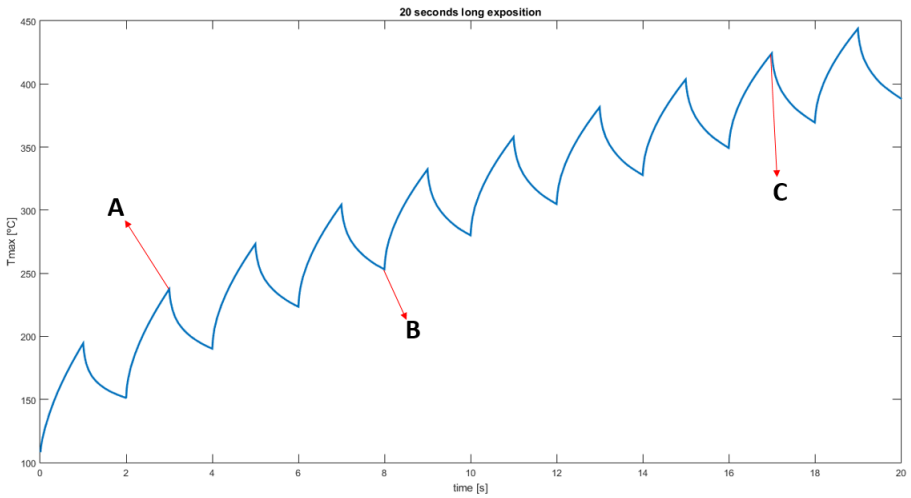

Figure 5.6 Cyclic operation of FILD 4 in intervals of one second reading at 3 cm insertion and one second cooling at parking position. FILD heat map for instants 3 s, 8 s and 17 s are also represented. Figures with the FILD heat map at times A, B and C are shown in figure 5.7.

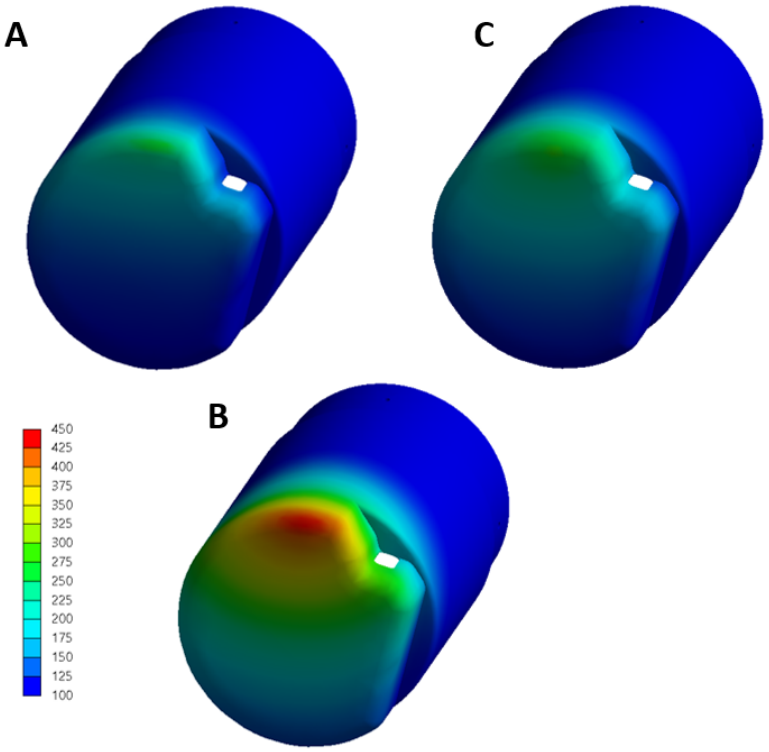

Figure 5.7 FILD 4 temperature profile during a 20 second cycle for times: a) 3 seconds with Tmax = 237.48ºC; b) 8 seconds with Tmax = 253.12ºC; c) 17 seconds with Tmax = 424.00ºC.

Second scenario (represented in figure 5.8) is a simpler one, just a 20 second long

exposition of FILD to plasma. Comparing both scenarios highlights the importance of a cyclic operation as the maximum temperature goes from 730ºC to 450ºC.

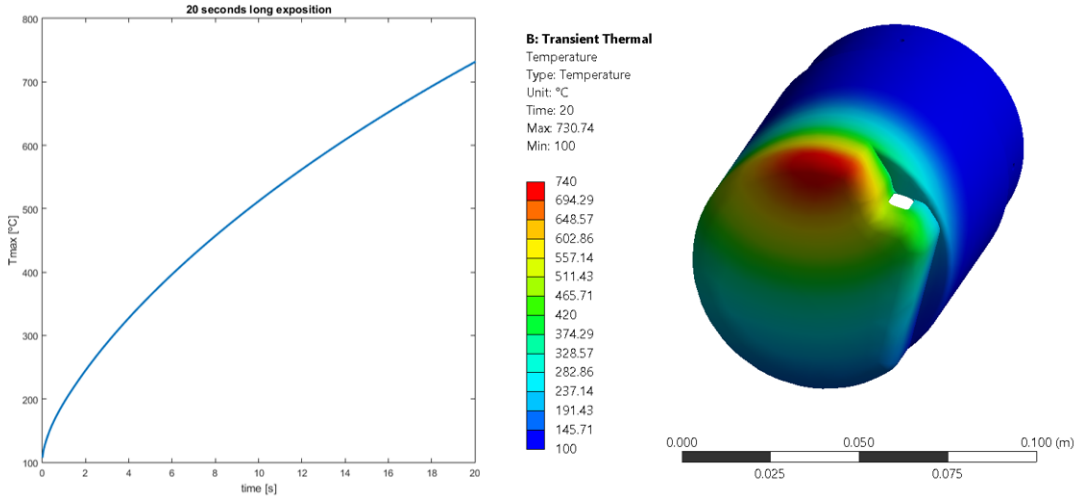

Figure 5.8 FILD 4 Tmax evolution during a 20 seconds exposition and temperature profile at the end of the simulation.

6 Conclusions and future work

Fast ions have shown to be a key element to achieve ignition, and therefore, for the success of nuclear fusion. Fast Ions Loss Detectors are designed to study their behavior in order to learn how to avoid their loses. A tool has been developed to analyze the thermal load one detector receives for a given position, in a determined Tokamak and plasma shot. For this purpose heat flux has been modeled using the cosine model, where heat flux is predominantly convective for PFC components such as FILD. To know which parts of the FILD are receiving heat flux via particle collision, a magnetic field line tracer has been developed due to these particles orbit being approximated by magnetic field lines. A series of optimization processes have been carried on in order to reduce long computational times: OcTree algorithm and preliminary analysis of the frontier between dry and wet zones were applied, these improvements mean an average reduction of the computational time of 43.76%.

An example of the temperature evolution over FILD head has been done in ANSYS software to demonstrate the applicability of the prior simulations.

The next step of this work is to add the developed code to FILDSIM [29]. FILDSIM is a software developed in MatLab focused in simulating FILD entirely. The aim of FILDSIM is to get the optimum position for a FILD for a series of constraints. Currently the software is prepared to give that optimum position but with the only goal of having the best readings, this would end with the device being seriously damaged by the intense heating there would be in that optimum position. But by adding the work developed here, a thermal criteria can be added as a limiting factor to the possible positions of a new FILD.

Thermal analysis can be further improved by calculating the stress distribution at the probe head caused by the thermal gradient. This will allow to assess the structural integrity of the probe head from static and dynamic (thermal fatigue) points of view.

Also extra work has to be done in order to further optimize the existing code. A way to achieve this may be by vectorizing when posible or by using the *Events* option inside the ode45 integrator to cut the integration whenever a collision is found, this would surely improve the computational time but is not expected to be groundbreaking.

Bibliography

[1] J. Freidberg *Plasma Physics and Fusion Energy* Cambridge, 2007

[2] S. Gasstone & R. H. Lovberg *Controlled Thermonuclear Reactions* Robert E. Krieger Publishing Company, 1975

[3] M. Vranic *Introduction to Inertial Confinement Fusion* Plasmasurf Summer School, Instituto de Plasmas e Fusão Nuclear Instituto Superior Técnico, Lisbon, Portugal, 2018

[4] Enciclopaedia Britannica *Ionization Energy* *https://www.britannica.com/science/ionization-energy*. Consulted July 2018

[5] V. Guerra *Introduction to plasma physics* Plasmasurf Summer School, Instituto de Plasmas e Fusão Nuclear Instituto Superior Técnico, Lisbon, Portugal, 2018

[6] Wikipedia *Guiding center* *https://en.wikipedia.org/wiki/Guiding_center*. Consulted July 2018

[7] A. Dinklage *Basic plasma physics and the motion of charged particles in magnetic fields* IPP Summer University, Max-Planck-Insititu für Plasmaphysik, Greifswald, Germany, 2016

[8] ITER *THE ITER TOKAMAK* *https://www.iter.org/mach*. Consulted July 2018

[9] B. Sieglin et al. *Investigation of scrape-off layer and divertor heat transport in ASDEX Upgrade L-mode* Plasma Physics and Contorlled Fusion, Volume 58, Number 5, 8 April 2016

[10] Max-Planck-Institut für Plasmaphysik *Introduction: The ASDEX Upgrade tokamak* *http://www.ipp.mpg.de/16208/einfuehrung*. Consulted July 2018

[11] ASDEX Upgrade *Detailed description of ASDEX Upgrade* *https://www.aug.ipp.mpg.de/wwwaug/documentation/physics/techdata.shtml*

[12] W.W. Heidbrink & G.J. Sadler *The behaviour of fast ions in Tokamak experiments* Nuclear Fusion, Volume 34, Number 4, 1994

[13] M. Rodriguez-Ramos *Calibración absoluta y aplicación de los detectores de pérdidas de iones rápidos basados en materiales centelleadores para dispositivos de fusión nuclear.* Doctoral Thesis at Physics Faculty at University of Seville, 2017

[14] J.F. Rivero-Rodriguez & M. Garcia-Munoz et al. *A rotary and reciprocating scintillator based fast-ion loss detector for the MAST-U tokamak* 22nd Topical Conference on High-Temperature Plasma Diagnostics, April 2018, Madison (USA)

[15] J.F. Rivero-Rodriguez *Implementation of a Fast-Ion Loss Detector in the MAST Upgrade Spherical Tokamak* Master Thesis at Engineering Superior School of Seville, 2017

[16] Plasma Science and Fusion Technology *Poloidal distribution of fast-ion losses http://www.psft.eu/research/diagnostics/fast-ion-loss-detector/*. Consulted July 2018

[17] P.A. Karasev *Triangle subdivide (vectorized/fast) https://es.mathworks.com/matlabcentral/fileexchange/25961-triangle-subdivide-vectorized-fast?focused=5140745&tab=function*. Consulted June 2018.

[18] M. Firdaouss & V. Riccardo et al. *Modelling of power deposition on the JET ITER like wall using the code PFCFLux* Journal of Nuclear Materials, Number 438 S536–S539, 2013

[19] T. Möller & B. Trumbore *Fast, Minimum Storage Ray/Triangle Intersection* Journal of Graphics Tools, 2(1):21–28, 1997

[20] J. Tuszynski *Triangle/Ray Intersection https://es.mathworks.com/matlabcentral/fileexchange/33073-triangle-ray-intersection*. Consulted February 2018

[21] Wikipedia *Barycentric coordinate system https://en.wikipedia.org/wiki/Barycentric_coordinate_system*. Consulted July 2018

[22] B. Sieglin *Experimental Investigation of Heat Transport and Divertor Loads of Fusion Plasma in All Metal ASDEX Upgrade and JET* Doctoral Dissertation at Max-Planck-Institut für Plasmaphysik, 2014

[23] R. Mitteau & A. Moal et al. *Heat flux deposition on plasma-facing components using a convective model with ripple and Shafranov shift* Journal of Nuclear Material, Number 266-269 S798-S803, 1999

[24] Y. Miyoshi & N. Asakura et al. *New model of plasma heat load on the first wall* Fusion Engineering and Design, Number 124 S267-S270, 2017

[25] C.S. Pitcher & P.C. Stangeby et al. *Plasma fluxes to surfaces for an oblique magnetic field* Journal of Nuclear Materials, Number 196-198 S241-S247, 1992

[26] P.C. Stangeby & C.S. Pitcher et al. *The nature of plasma fluxes to surfaces nearly tangential to the magnetic field* Nuclear Fusion , 32 S2079, 1992

[27] M.Firdaouss & T. Batal et al. *Heat flux depositions on the WEST divertor and first wall components* Fusion Engineering and Design, Number 98-99 S1294-S1298,2015

[28] A. Zaffora *Mappin External Data on Structural Mesh* ANSYS Italy, 2013

[29] J. Galdon *Velocity-space sensitivity and tomography of scintillator-based fast-ion loss detectors* Plasma Physics and Controlled Fusion, Number 60 S10, 2018